IEEE Access
Multidisciplinary | Rapid Review | Open Access Journal

Received July 24, 2019, accepted August 11, 2019, date of publication August 23, 2019, date of current version September 10, 2019.

Digital Object Identifier 10.1109/ACCESS.2019.2937100

Comprehensive Studies on Operational Principles for Maximum Power Point Tracking in Photovoltaic Systems

XINGSHUO LI[1], (Student Member, IEEE), QI WANG[1], HUIQING WEN[2], (Senior Member, IEEE), AND WEIDONG XIAO[3], (Senior Member, IEEE)

[1]School of Electrical and Automation Engineering, Nanjing Normal University, Nanjing 210023, China
[2]Department of Electrical and Electronic Engineering, Xian Jiaotong-Liverpool University, Suzhou 215123, China
[3]School of Electrical and Information Engineering, University of Sydney, Sydney, NSW 2006, Australia

Corresponding author: Qi Wang (wangqi@njnu.edu.cn)

ABSTRACT Maximum power point tracking (MPPT) is essential in Photovoltaic (PV) systems, which has drawn significant research effort in the past. The operation is to adjust the power interfaces so that the operating characteristics of the consumption and the PV generator match at the ideal level in term of generation. A comprehensive review is essential to help readers understand the latest developments and inform research directions. Unlike the other review papers, this paper focuses on the operational principles of MPPT methods. Therefore, a different review angle is presented in this paper to provide a clear image of the technology of MPPT.

INDEX TERMS Photovoltaic (PV) system, maximum power point tracking (MPPT), review.

I. INTRODUCTION

Among renewable energies, solar Photovoltaic (PV) generation increases significantly in the past. According to European Photovoltaic Industry Association (EPIA), 98 GW of Photovoltaic (PV) capacity was installed globally in 2017 [1]. Besides, PV alone experienced more net power generating capacity added than coal, natural gas and nuclear combined [1]. However, the government policy and subsidies are still the major motivation for the PV development [2]. Furthermore, unlike the fossil fuels energies, the output power of the PV system are various and dependent on different working conditions.

The electrical characteristics of a PV module under different weather conditions are plotted in FIGURE 1. The I-V and P-V curves show the maximum power point (MPP), which represents the maximum power output that can be extracted from the PV generator under certain environmental conditions [3]. Therefore, maximum power point tracking (MPPT) becomes essential for PV power applications.

Excessive number of review papers on MPPT methods have been reported in recent years [4]–[11]. However, only the generalized overview and the key findings of these methods are reviewed and compared, such as cost, efficiency, complexity, hardware dependency and so on. The operational principles of these methods are not comprehensively explored and discussed. Actually, many so called ''improved'' or ''enhanced'' methods are originated from the conventional ones. Furthermore, the relevance and evolution among the MPPT methods are generally ignored. The exploration on how to modify the conventional methods being more effective and efficient is more interested by researchers and engineers working in PV-based power systems.

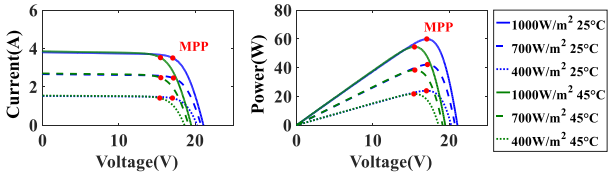

FIGURE 1. PV characteristics under different weather conditions.

In this paper, the MPPT methods are reviewed in a different angle. Firstly, the scope of reviewed MPPT methods is defined. Then, the operational principles of the typical MPPT methods are reviewed, classified and analyzed in details. The relevance and evolution among MPPT methods are also discussed and explored. Finally, the reviewed MPPT methods will be summarized and possible improvement suggestions are also given.

The associate editor coordinating the review of this article and approving it for publication was Xianming Ye.

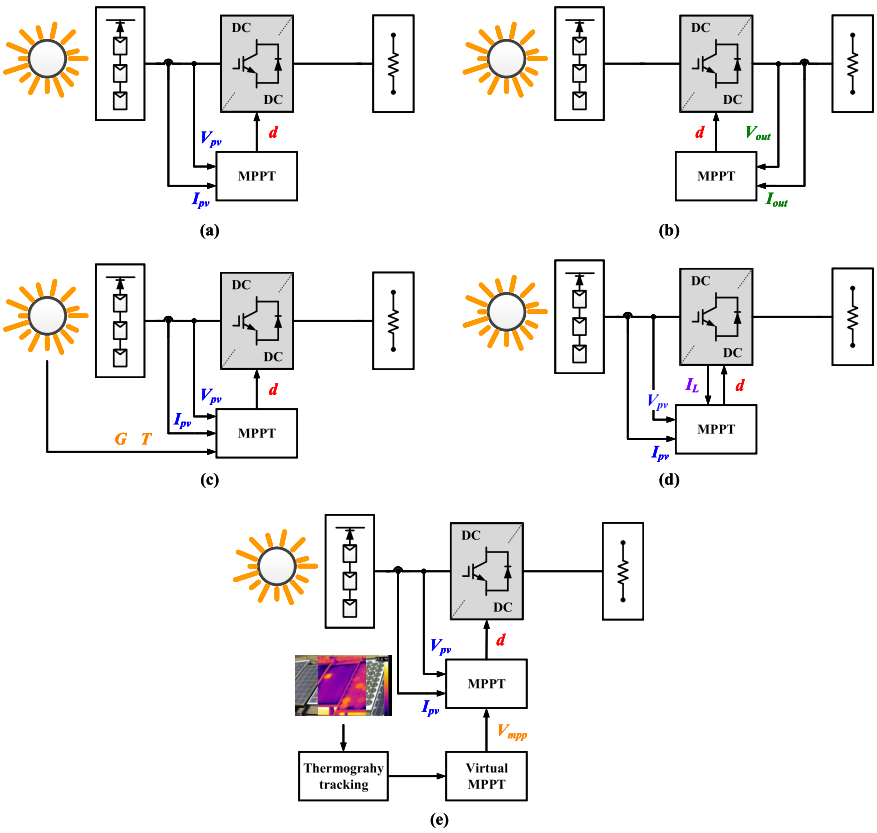

FIGURE 2. Different MPPT implementations. (a) PV-side sensors. (b) Output sensors. (c) Additional solar irradiance and/or temperature sensors. (d) Additional inductor current sensors. (e) Thermography camera.

II. INTRODUCTION OF PV SYSTEMS

A. MPPT IMPLEMENTATIONS

Based on the locations of sensors and the type of sensors, there are five different MPPT implementations, as shown in FIGURE 2. FIGURE 2 (a) shows the most common implementation where the PV-side current sensor and/or voltage sensor are required. It should be noted that the majority of available MPPT methods are based on this implementation [4]. By contrast, the output voltage sensor and/or current sensor can be also used to realise the MPPT, as shown in FIGURE 2 (b). However, this kind of implementation cannot guarantee the true MPPT [4].

Additional sensors are also used in some MPPT implementations. As shown in FIGURE 2 (c), the solar irradiance and/or temperature are measured and sent to the MPPT controller. Generally, only the model-based methods require this implementation [12]. Besides, sliding mode (SM) control requires to measure the inductor current [13], as shown in FIGURE 2 (d). In recent years, the thermography-based virtual MPPT is proposed in [14] where a thermography camera is used to assist the MPPT, as shown in FIGURE 2 (e). Although the effectiveness of these implementations with additional sensors are validated, the cost and complexity of them are generally high due to more sensors used.

As aforementioned discussion, the MPPT implementation with the PV-side sensors is the most generic MPTT algorithm. Therefore, only the MPPT methods based on this implementation are studied in this paper.

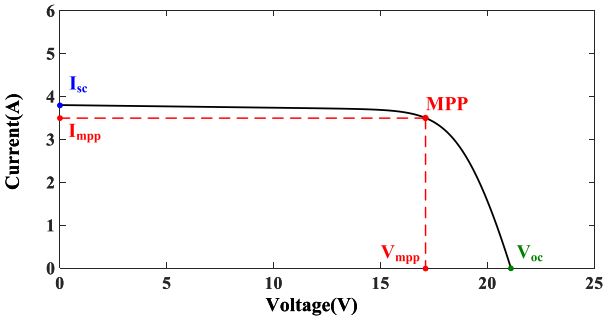

FIGURE 3. I-V curve of the PV characteristics.

B. PV OUTPUT CHARACTERISTICS

I-V curve is usually used to illustrate the outputs of PV characteristics [15], [16]. Generally, there are five main parameters to demonstrate the PV output characteristics, such as such as open-circuit voltage V_{oc}, short-circuit currentI_{sc}, voltage at the MPP V_{mpp}, current at the MPP I_{mpp} and power at the MPP P_{mpp}, as shown in FIGURE 3.

The PV manufacturing data sheet normally provides these parameters at standard test condition (STC), where the solar irradiance is at $1000W/m^2$ and the cell temperature is at 25°.

TABLE 1. Main product parameters of the PV module MSX-60W.

Parameter	Symbol	Value
Maximum power	P_{mpp}	$60W$
Voltage at maximum power	V_{mpp}	$17.1V$
Current at maximum power	I_{mpp}	$3.5A$
Open-circuit voltage	V_{oc}	$21.1V$
Short-circuit current	I_{sc}	$3.8A$
Temperature coefficient of V_{oc}	K_v	$-80mV/°C$
Temperature coefficient of I_{sc}	K_i	$0.065\%/°C$

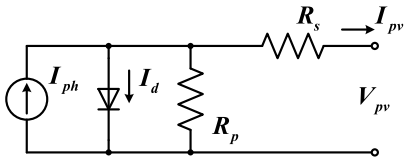

FIGURE 4. Equivalent circuit of single-diode model (SDM).

In this paper, the Solarex MSX-60W is chosen and its electrical characteristics are shown in TABLE 1.

An equivalent circuits model is usually used to represent the PV characteristics. Single-diode model (SDM) is widely used in the previous research [17].

As shown in FIGURE 4, the current-voltage (I-V) characteristics according to the SDM model are expressed as

$$I_{pv} = I_{ph} - I_d - \frac{V_d}{R_p} \tag{1}$$

where I_{ph} represents the photon current. I_d is Shockley diode equation, which can be expressed as:

$$I_d = I_s\left[e^{\frac{V_d}{\eta V_t}} - 1\right] \tag{2}$$

where I_s is the reverse saturation current of the diode and η is the diode ideality factor. V_d and V_t refer to

$$V_d = V_{pv} + I_{pv}R_s \tag{3}$$

$$V_t = \frac{kT}{q} \tag{4}$$

where V_t is the thermal voltage, k is Boltzmann constant ($1.38 \times 10^{-23}J/K$), T(in Kelvin) is the temperature of the p–n junction, and q is the electron charge ($1.602 \times 10^{-19}C$). Substitute (2-4) into (1), it can be rearranged as:

$$I_{pv} = I_{ph} - I_s\left[e^{\frac{V_{pv}+I_{pv}R_s}{\eta V_t}} - 1\right] - \frac{V_{pv} + I_{pv}R_s}{R_p} \tag{5}$$

Since there are five unknown parameters in (5), this SDM is also known as five-parameter PV model [17].

In practice, the PV source generally consists of several PV modules, which are connected in series and formed into a PV string. When the PV string is under the uniform condition, only one peak, namely maximum power point (MPP), is displayed on its I-V and P-V curve, as shown in FIGURE 5. However, when the PV string is under the partial shading condition (PSC), there are multiple peaks, namely one global MPP (GMPP) and several local MPPs (LMPP), on the I-V and P-V curve. Therefore, the global maximum power point tracking (GMPPT) is also essential [18].

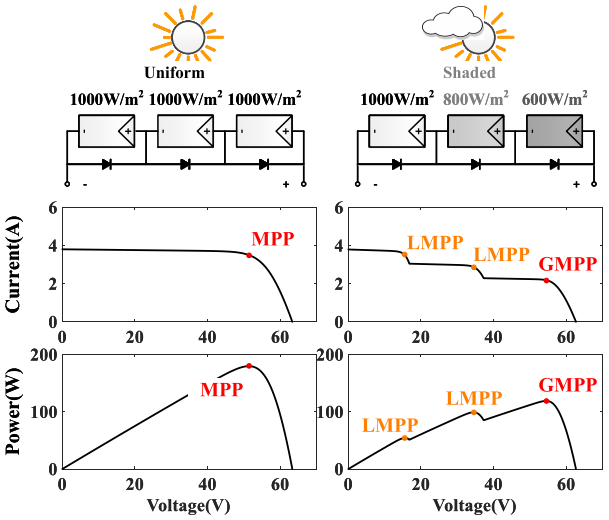

FIGURE 5. PV string characteristics under uniform condition and partial shading condition.

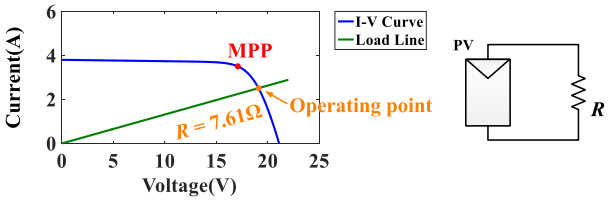

FIGURE 6. Impedance match for the MPPT: Direct load match.

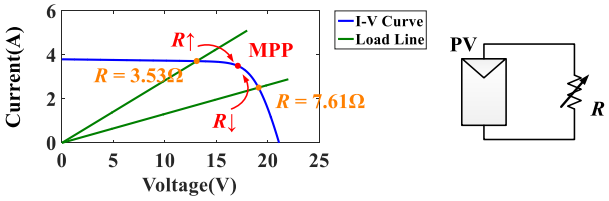

FIGURE 7. Impedance match for the MPPT: Variable load match.

In this paper, only the MPPT methods are reviewed. Therefore, the GMPPT methods, such as segmental search methods [19]–[21], power increment methods [22], [23] load line methods [24], [25] and $0.8V_{oc}$ model methods [26]–[29] will not be reviewed.

III. OPERATIONAL PRINCIPLE OF MAXIMUM POWER POINT TRACKING METHODS

The principle behind MPPT is the impedance match between the PV generator output and the load condition [16]. Assuming that a PV panel is directly connected with a resistor load, which is shown in FIGURE 6. The operating point is plotted as the intersection between the I–V curve and load line when the resistance is 7.61Ω. If the PV module is connected with a variable resistor, the operating point can move alone the PV I–V curve by adjusting the value of the resistor, as shown in FIGURE 7.

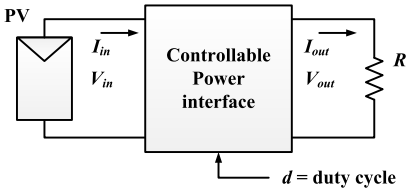

FIGURE 8. Controlled power interface between the PV generator and load.

Generally, the load requires either constant current or voltage, so the load impedance cannot always be adjusted for the MPPT. Therefore, a controlled power interface, as shown in FIGURE 8, is connected between the PV generator and load to realise an equivalent resistance to match the MPP. Assuming that a DC-DC converter is used as the controlled power interface, where I_{in} and V_{in} are input current and voltage, respectively; I_{out} and V_{out} are output current and voltage, respectively; d refers to the duty cycle of the DC-DC converter.

Assuming that the DC-DC converter is ideal, the mathematical expression for the DC-DC converter can be given by:

$$V_{in} = \frac{V_{out}}{M(d)} \tag{6}$$

$$I_{in} = M(d) \cdot I_{out} \tag{7}$$

where $M(d)$ is the voltage conversion ratio. Divide (6) by (7), it can be derived as:

$$R_{in} = \frac{V_{in}}{I_{in}} = \frac{V_{out}/M(d)}{M(d) \cdot I_{out}} = \frac{1}{M(d)^2} \cdot \frac{V_{out}}{I_{out}} = \frac{R_{out}}{M(d)^2} \tag{8}$$

where R_{in} refers to the input resistance and R_{out} refers to the output resistance. Since the input of the DC-DC converter is the PV source, (8) can be rewritten as:

$$R_{pv} = \frac{R_{load}}{M(d)^2} \tag{9}$$

where R_{pv} refers to the equivalent resistance of the PV source, and R_{load} represents the load resistance.

It should be noted that there are different $M(d)$ for different DC-DC converters, as summarized in TABLE 2. Taking the boost converter as an example, its $M(d)$ is given as below:

$$M(d) = \frac{1}{1-d} \tag{10}$$

Substitute (10) into (9), it can be derived as:

$$R_{pv} = R_{load}(1-d)^2 \tag{11}$$

From discussion above, the left terms in (11) can be regarded as the equivalent resistance.

From discussion above, the left terms in (11) can be regarded as the equivalent resistance. By adjusting the value of d, the MPP can be located.

TABLE 2. Summary of $M(d)$ and R_{pv} for different DC-DC converters.

Converter	$M(d)$	R_{pv}
Buck	d	$\frac{1}{d^2}R_{load}$
Boost	$\frac{1}{1-d}$	$(1-d)^2 R_{load}$
Buck-Boost	$-\frac{d}{1-d}$	$\frac{(1-d)^2}{d^2}R_{load}$
Cuk	$-\frac{d}{1-d}$	$\frac{(1-d)^2}{d^2}R_{load}$
SEPIC	$\frac{d}{1-d}$	$\frac{(1-d)^2}{d^2}R_{load}$

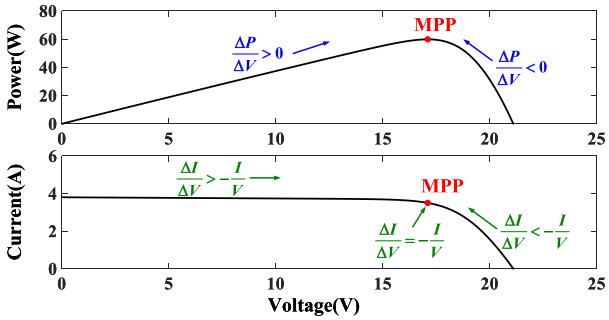

FIGURE 9. Determination of the perturbation direction for the P&O and INC method.

A. PERTURB AND OBSERVE AND INCREMENTAL CONDUCTANCE

Perturb and observe (P&O) and incremental conductance (INC) are the most popular MPPT methods [30]–[34]. The basic operational principles of the P&O and the INC method are demonstrated in FIGURE 9. The direction of voltage perturbation for the P&O method is determined by

$$V_{ref} = \begin{cases} V + V_{step}, & \frac{\Delta P}{\Delta V} > 0 \quad (12a) \\ V - V_{step}, & \frac{\Delta P}{\Delta V} < 0 \quad (12b) \end{cases}$$

where ΔP, ΔV and ΔI refer to the changes in power, voltage and current, respectively, V_{step} refers to the voltage step size. At the meanwhile, the direction of voltage perturbation for the INC method is determined by

$$V_{ref} = \begin{cases} V + V_{step}, & \frac{\Delta I}{\Delta V} > -\frac{I}{V} \quad (13a) \\ V + 0, & \frac{\Delta I}{\Delta V} = -\frac{I}{V} \quad (13b) \\ V - V_{step}, & \frac{\Delta I}{\Delta V} < -\frac{I}{V} \quad (13c) \end{cases}$$

It should be noted that (13b) is unlikely satisfied in practice due to digital resolution.

FIGURE 10 demonstrates the typical behaviours of the P&O and the INC method during the steady-state stage. Point A and C refer to the location on left and right of the MPP, respectively. Point B refers to the nearly coincident location of the MPP. As shown in FIGURE 10, the operating point

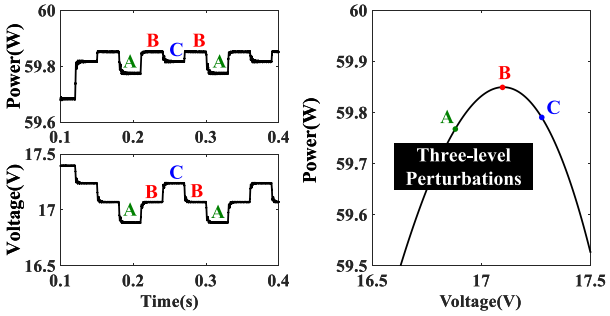

FIGURE 10. Steady-state three-level oscillations around the MPP.

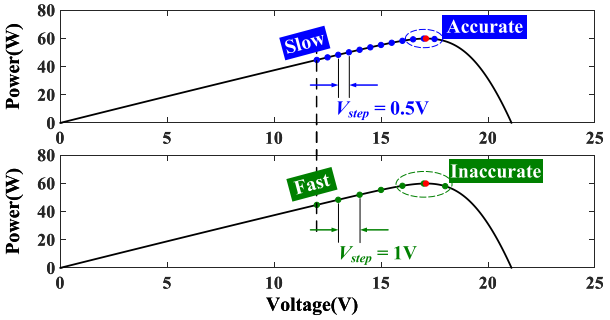

FIGURE 11. Different fixed-step sizes for the P&O and INC method.

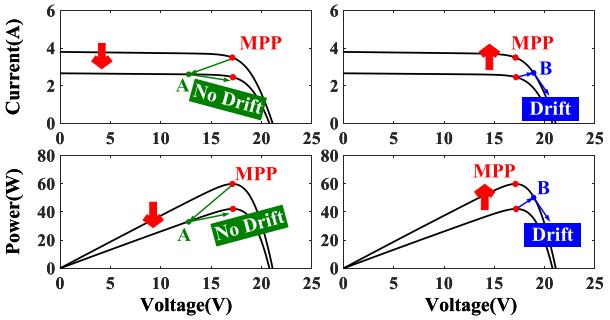

FIGURE 12. Movement of the operating point under the sudden irradiance changes.

repeats the process following the trajectory (A) → (B) → (C) → (B) → (A). Due to three power/voltage levels in the steady-state stage, this behaviour is famous as three-level oscillations.

Fixed-step size is generally used for the P&O and INC methods. However, simultaneous optimization of the steady-state and dynamic performance is very difficult. As demonstrated in FIGURE 11, the methods with a larger step size (i.e., 1V) have a fast tracking speed in the dynamic stage. By contrast, the methods with a smaller step size (i.e., 0.5V) have a small oscillations in the steady-state stage.

In most of cases, both of P&O and INC method are able to make a correct movement towards the MPP. However, a wrong movement is also possible to be made under a sudden increase in solar irradiance. As shown in FIGURE 12, the operating point moves from the MPP to point B when the solar irradiance is increased. At this time, (12a) and (13a) are satisfied and the voltage is perturbed to the left. Then, the

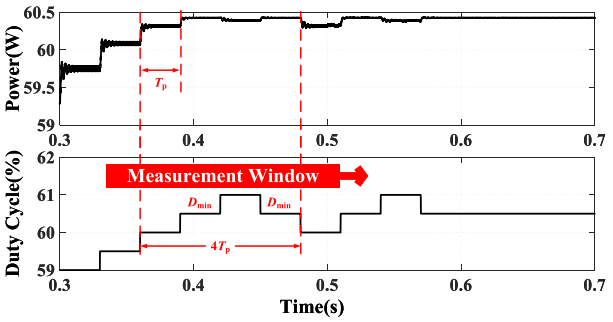

FIGURE 13. Operational principle of zero-oscillations methods in.

wrong movement is made by both of P&O and INC method. As a consequence, the operating point is drifted away from the MPP. It should be also noted that there is no drift happened if the solar irradiance is decreased.

From aforementioned discussion, there are three drawbacks for the P&O and INC method:

- Steady-state oscillations;
- Simultaneous optimization;
- Drift conditions.

In order to solve these problems, many modified or enhanced P&O and INC methods are proposed and will be discussed in the following sections.

1) ZERO-OSCILLATIONS METHODS

Zero-oscillations methods are proposed to remove the oscillations in recent years. Generally, there are two ways to realise it. One way is to use a permitted error e_{th} by rewriting (13b) as [35]

$$V_{ref} = V + 0, \quad |I + V\frac{\Delta I}{\Delta V}| < e_{th} \tag{14}$$

Although this method is very simple, the problem is how to tune the value of e_{th}.

The second way is more popular and its basic idea is to find the middle level from the three-level oscillations. Various ways to find the middle level are reported in [36], [37]. Here, one solution in is demonstrated in FIGURE 13. A measurement window with a time period $4T_p$ is defined, where T_p refers to MPPT perturbation rate. If two middle level D_{mid} are found in the measurement window, a variable *counter* is counted. As the measurement window is moving, when *counter* is reached to 4, the operating point will be maintained at D_{mid}. As a consequence, there is no more oscillation.

2) VARIABLE-STEP SIZE METHODS

Generally, the variable-step size is used to solve the trade-off between the steady-state and dynamic performance. The step size can be automatically adjusted by the P-V curve gradient [38]–[41], P-I curve gradient [42] and P-D curve gradient [43].

Among these methods, the P-V curve gradient is the most commonly used. Thus, the step size X_{step} can be expressed

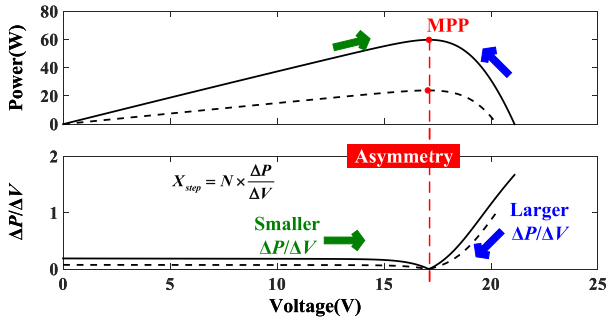

FIGURE 14. Asymmetrical variable-step size method.

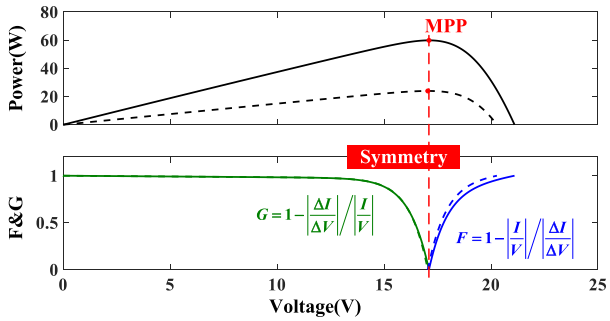

FIGURE 15. Symmetrical variable-step size method.

as below:

$$X_{step} = N \times \left|\frac{\Delta P}{\Delta V}\right| \tag{15}$$

where X_{step} are commonly used as duty cycle or voltage, N is a fixed scaling factor adjusted at the sampling period to regulate the step size [38].

The term $\Delta P/\Delta V$ is highly asymmetrical relative to the MPP, as demonstrated in FIGURE 14. Consequently, it will result in a larger value in the right-hand side of the MPP and a smaller step size in the left-hand. Therefore, the value of N has to be used and tuned to balance this right-and-left asymmetry of the gradient of P-V curve. However, this value of N may not be suitable for all of the weather conditions. For example, this asymmetry becomes more significant, when the solar irradiance decreases, as marked in black dash lines in FIGURE 14.

Unlike the aforementioned asymmetrical variable-step size MPPT methods, a symmetrical variable-step size MPPT method is proposed in [44]. This method uses two parameters, namely F and G, to regulate the step size, as shown below:

$$\begin{cases} G = 1 - \left|\frac{\Delta I}{\Delta V}\right| \Big/ \left|\frac{I}{V}\right|, & \text{Left of MPP} \quad (16a) \\ F = 1 - \left|\frac{I}{V}\right| \Big/ \left|\frac{\Delta I}{\Delta V}\right|, & \text{Right of MPP} \quad (16b) \end{cases}$$

Then, the step size X_{step} can be derived as below:

$$X_{step} = \begin{cases} \Delta N \times G, & \text{Left of MPP} \quad (17a) \\ \Delta N \times F, & \text{Right of MPP} \quad (17b) \end{cases}$$

As shown in FIGURE 15, the curve of F and the curve of G are highly symmetrical relative to the MPP. Furthermore, even if the weather condition changes, such as irradiance decreases, the symmetry between F and G is still maintained. Therefore, this symmetrical variable-step size MPPT method is more adaptive than the asymmetrical ones.

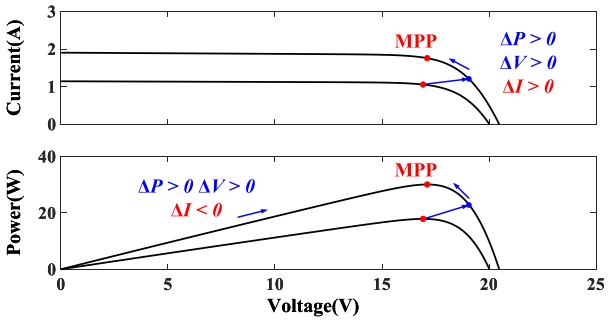

FIGURE 16. Movement of the operating point for the drift-free method.

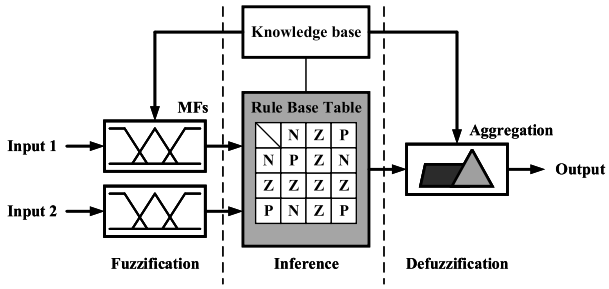

FIGURE 17. Structure of the fuzzy logic controller.

3) DRIFT-FREE METHODS

In order to avoid the drift condition, there are many drift-free methods to solve this, such as setting a constraint on step size [30] or power threshold ΔP [45]. However, it is difficult to tune these parameters, and they may not be suitable for all of the weather conditions.

As a matter of fact, another solution has been proposed in [35], [46] by incorporating the information of ΔI in the decision part. Since the drift condition is normally happened during the irradiance increases, it is only required to incorporate ΔI in (12a) and (13a) as below

$$V_{ref} = \begin{cases} V - V_{step}, & \Delta I > 0 \quad (18a) \\ V + V_{step}, & \Delta I < 0 \quad (18b) \end{cases}$$

FIGURE 16 demonstrates the movement of operating point for the drift-free method. With the aid of ΔI incorporation, the drift-free method can successfully eliminate the drift condition. Besides, the incorporation of ΔI will not result in drift condition if the solar irradiance is not suddenly increased.

B. FUZZY LOGIC CONTROL

Fuzzy Logic Control (FLC) is another popular MPPT method [47]–[53]. Generally, there are three stages for the the FLC method, which is shown in FIGURE 17. In the first stage, the numerical input variables are converted into equivalent linguistic variables as input fuzzy sets. In the second stage, the input fuzzy sets are converted into output fuzzy

sets through the inference with the fuzzy rule base table. Finally, the output fuzzy sets are converted into the numerical variables as the output.

To be more specific, the input variables could be the error E and the change in error ΔE, which can be calculated by the gradient of P-V curve [48] as follow:

$$E(k) = \frac{P(k) - P(k-1)}{V(k) - V(k-1)} \tag{19}$$

$$\Delta E(k) = E(k) - E(k-1) \tag{20}$$

where $P(k)$ and $V(k)$ are PV output power and voltage respectively at time k.

Five fuzzy levels are used for membership functions (MFs), such as NB (negative big), NS (negative small), ZE (zero), PS (positive small), and PB (positive big). Since the $\Delta P/\Delta V$ curve is highly asymmetric at the MPP, as illustrated in FIGURE 14, the MFs of $E(k)$ with five fuzzy levels have to be carefully designed in order to ensure the symmetric feature of the output [51]. As a result, the designed MFs with five fuzzy levels are demonstrated in FIGURE 18, which shows that the output variable is symmetric around zero. These specific 25 fuzzy rules are also clearly shown in TABLE 3.

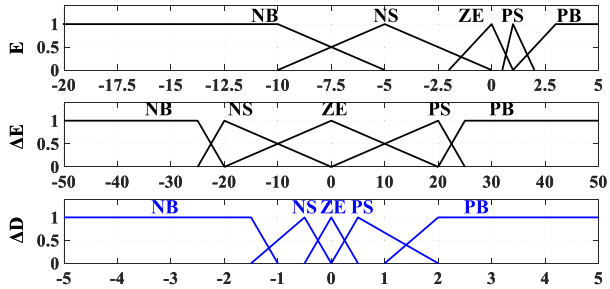

FIGURE 18. Structure of the fuzzy logic controller.

TABLE 3. Rule base table with five fuzzy levels.

E \ ΔE	NB	NS	ZE	PS	PB
NB	PB	PB	PS	PB	PB
NS	PB	PS	PS	PS	PB
ZE	NS	NS	ZE	PS	PS
PS	NB	NS	NS	NS	NB
PB	NB	NB	NS	NB	NB

The FLC method generally exhibits a good performance under varying weather conditions. However, the MFs and fuzzy rules are heavily relied on the designer's knowledge of the system. Therefore, how to reduce this dependence is the main motivation to modify the FLC method. Generally, there are two ways to achieve it:

- Simplify the design;
- Optimize the parameters.

1) DESIGN SIMPLIFICATION

In order to reduce the dependence on designer's knowledge, some MPPT methods, such as the P&O method, are integrated into the FLC to achieve simple design of MFs and fuzzy rules. The basic idea is how to reduce the number of fuzzy rules.

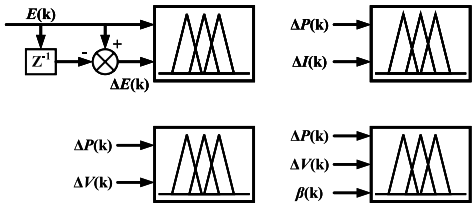

FIGURE 19. Integration with other MPPT methods.

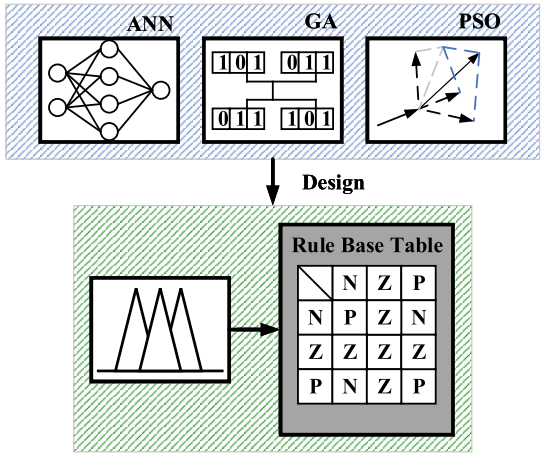

FIGURE 20. Integration with artificial intelligence algorithms.

For instance, ΔP and ΔI can be used as the input variables instead of ΔE and $E(k)$ [47], as shown in FIGURE 19. The corresponding MFs and fuzzy rules can be designed by translating the P&O method. Thus, the number of fuzzy rules can be reduced into 16. In [54], a three input variables, ΔP, ΔV and β, are used and the number of fuzzy rules is reduced into 11.

2) PARAMETER OPTIMIZATION

Integration with artificial intelligence (AI) algorithms is another way to reduce the dependence on designer's knowledge. This approach makes the FLC method more complex rather than simpler.

As shown in FIGURE 20, the AI algorithms, such as artificial neural network (ANN) [55]–[58], genetic algorithm (GA) [59], [60] and particle swarm optimization (PSO) [61], [62], are used to optimize the parameters of MFs and fuzzy rules. Since optimum MFs and fuzzy rules are tuned by these artificial intelligence algorithms, the dependence on designer's knowledge for the FLC can be reduced. Nevertheless, it is required additional knowledge on these artificial intelligence algorithms.

C. CURVE-FITTING

Curve-fitting methods are generally used for PV modelling rather than MPPT. Besides, some special points like open-circuit voltage and short-circuit current are required to fit the

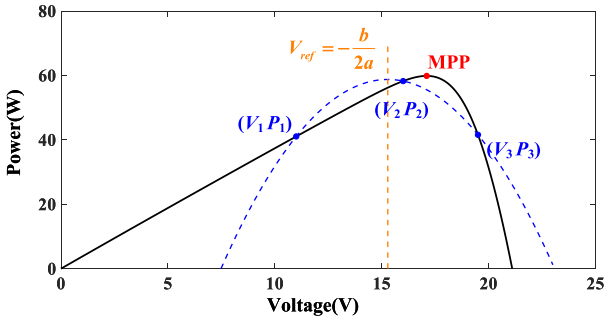

FIGURE 21. Approximation of the P-V characteristics by a parabolic curve.

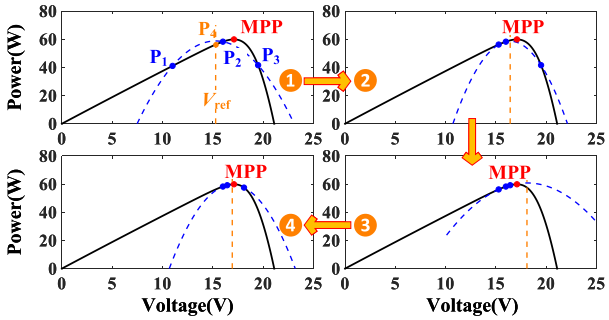

FIGURE 22. Operational principle of the parabolic prediction method.

P-V curves [63], [64]. However, these special points are not easily obtained in the practice. Therefore, how to fit the P-V curves without using these special points is a problem.

1) PARABOLIC PREDICTION

Parabolic prediction method is based on the fact that P-V curves can be fitted as a parabolic curve [65]–[67]. A quadratic polynomial can be written as:

$$P_{pv} = aV_{pv}^2 + bV_{pv} + c \tag{21}$$

Assuming that three points in the P-V curve are known, namely (V_1 P_1), (V_2 P_2) and (V_3 P_3). The parameters a, b and c can be obtained:

$$a = \frac{P1}{\Delta V12 \cdot \Delta V13} + \frac{P2}{\Delta V21 \cdot \Delta V23} + \frac{P3}{\Delta V31 \cdot \Delta V32} \tag{22}$$

$$b = -\frac{P1(V2+V3)}{\Delta V12 \cdot \Delta V13} + \frac{P2(V1+V3)}{\Delta V21 \cdot \Delta V23} + \frac{P3(V1+V2)}{\Delta V31 \cdot \Delta V32} \tag{23}$$

$$c = \frac{P1 \cdot V2 \cdot V3}{\Delta V12 \cdot \Delta V13} + \frac{P2 \cdot V1 \cdot V3}{\Delta V21 \cdot \Delta V23} + \frac{P3 \cdot V1 \cdot V2}{\Delta V31 \cdot \Delta V32} \tag{24}$$

where

$$\Delta V_{ij} = V_i - V_j, \quad i, j = 1, 2, 3. \tag{25}$$

The iteration process for the parabolic prediction method is demonstrated in FIGURE 22. Initially, three points on the P-V curve are measured and a, b and c can be obtained. Then, the operating point will move to the reference voltage V_{ref}:

$$V_{ref} = -\frac{b}{2a} \tag{26}$$

After the operating point moves to the new position, the power value at this new position P_4 will be compared with P_1, P_2 and P_3. The lowest power point of the four will be dropped and the rest of the three points will be used for the next iteration. This iteration will be continuously repeated until the MPP is reached.

2) PARAMETER ESTIMATION

Parameter estimation method is usually used to extract the physical parameters, such as R_s, R_p and even the solar irradiance and temperature [68]. Recently, some new parameter estimation methods are proposed, which requires several pairs of voltage and current values [69], [70].

Taking [70] as an example, equation (1) is firstly simplified as (27). The details of this simplification can be found in [70].

$$I = \alpha + \beta V^{\gamma} \tag{27}$$

where α, β and γ are constants and can be calculate by only three pairs of voltage and current values namely (v_1 i_1), (v_2 i_2) and (v_3 i_3). Taking the first derivative of (27), it can be written as:

$$I' = \beta.\gamma.V^{(\gamma-1)} \tag{28}$$

The means of the three pairs of voltage and current values can be written as

$$I'_{12} = \frac{i_2 - i_1}{v_2 - v_1} \quad I'_{23} = \frac{i_3 - i_2}{v_3 - v_2} \tag{29}$$

$$V_{12} = \frac{v_1 + v_2}{2} \quad V_{23} = \frac{v_2 + v_3}{2} \tag{30}$$

Combining (28) with (29) and (30) yields

$$I'_{12} = \beta.V_{12}^{(\gamma-1)} \quad I'_{23} = \beta.V_{23}^{(\gamma-1)} \tag{31}$$

Then, γ can be calculated as

$$\gamma = \frac{\ln(\frac{I'_{12}}{I'_{23}})}{\ln(\frac{V_{12}}{V_{23}})} + 1 \tag{32}$$

Combining (31) with (32) yields

$$\beta = \frac{I'_{12}}{\gamma.V_{12}^{(\gamma-1)}} \tag{33}$$

Finally, α can be obtained

$$\alpha = I_1 - \beta.V_1^{\gamma} \tag{34}$$

After α, β and γ are obtained, the estimated I-V curve as well as the estimated MPP can be obtained too. As illustrated in FIGURE 23, it can be seen that the estimated MPP is very close to the actual MPP.

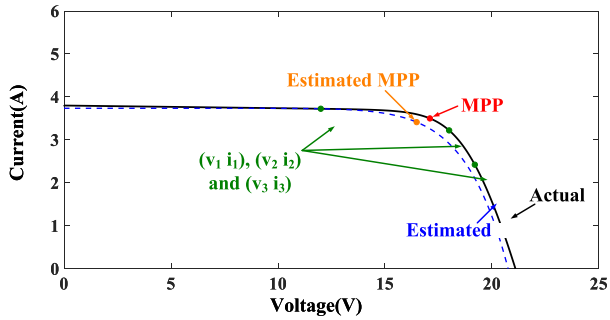

FIGURE 23. Operational principle of the parameter estimation method in [70].

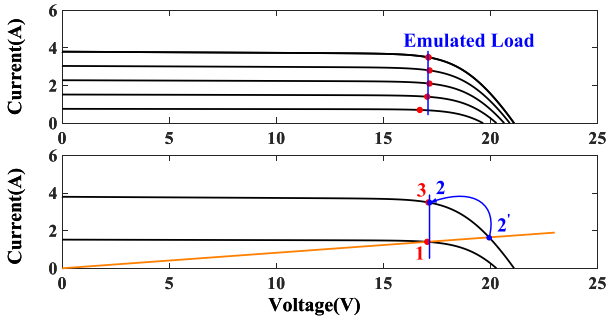

FIGURE 24. Basic operational principle of the MPP-Locus method in [71].

D. MPP-LOCUS METHOD

The MPP-Locus method is firstly proposed by Sokolov and Shmilovitz [71]. The basic operational principle of this method is demonstrated in FIGURE 24.

As shown in FIGURE 24, the locations of MPPs under different solar irradiance are nearly to form a straight line, which is expressed as

$$V_{ref} = V - rI \tag{35}$$

where V_{ref} refers to the emulated load tuned by an appropriate gain r. Based on (35), the operating point can be always maintained on this straight line.

As shown in FIGURE 24, when the weather condition is changed, the operating point moves from the point 1 to 2′. Then, the MPP-Locus method will force the operating point directly move to point 2. Finally, the P&O method is used to exactly locate the MPP position.

The MPP-Locus method in [71] shows a good result under dynamic weather conditions. However, only preliminary results are provided and the tracking procedure is not specific enough. Therefore, there are two ways to improve the insufficiencies above:

- How to precisely express V_{ref};
- How to maintain the operation point at V_{ref}.

1) EXPRESSION OF VOLTAGE LINE

In [72], V_{ref} can be analytically expressed as

$$V_{ref} = kI_{mpp} + V_{DO} \tag{36}$$

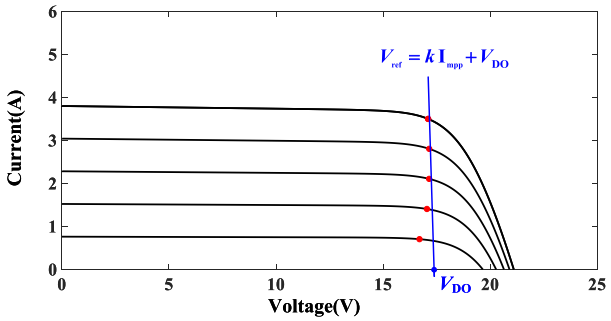

FIGURE 25. Voltage line expressed by [72].

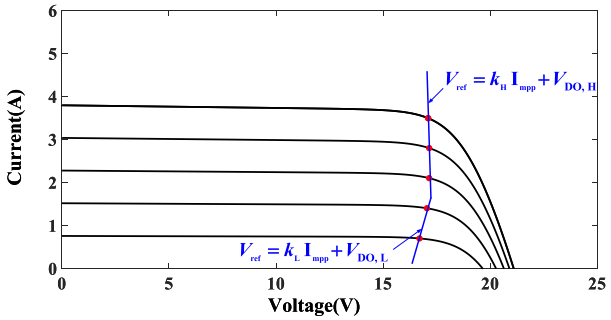

FIGURE 26. Two voltage lines expressed by [73].

where k is a constant value, V_{DO} is a defined term called Differential Offset Voltage. V_{DO} in (36) can be calculated as

$$V_{DO} = V^*_{oc} - V^*_{ov} - \eta V_t I^*_{mpp} \tag{37}$$

where V^*_{oc}, V^*_{ov} and I^*_{mpp} refer to the corresponding values at defined condition in [72]. V^*_{ov} can be calculated as

$$V^*_{ov} = \eta V_t \ln(1 + V^*_{mpp}/(\eta V_t)) \tag{38}$$

As shown in FIGURE 25, the voltage line can be expressed for most of the MPP locus when the solar irradiance is high. However, (36) can not be expressed the MPP locus when the solar irradiance is low.

In order to improve this problem, an additional line is employed to express the MPP locus under low solar irradiance [73]. Thus, (36) can be rewritten as

$$V_{ref} = \begin{cases} k_H I_{mpp} + V_{DO,H} & \text{(39a)} \\ k_L I_{mpp} + V_{DO,L} & \text{(39b)} \end{cases}$$

where k_H and k_L refer to the constant values under high and low solar irradiance, respectively, $V_{DO,H}$ and $V_{DO,L}$ refer to V_{DO} under high and low solar irradiance, respectively.

2) MAINTAIN AT VOLTAGE LINE

The operational principle of the improved MPP-locus method in [74] is demonstrated in FIGURE 27. The key of this method is how to determine I_{mpp} when the solar irradiance is changed.

When the solar irradiance is decreased, the operating point moves from MPP_1 to point A (V_1, I_1). At this time, I_{mpp} can be approximately equal to I_1 and V_{ref} can be calculated by (36). Then, the operating point will be forced to B, which is very

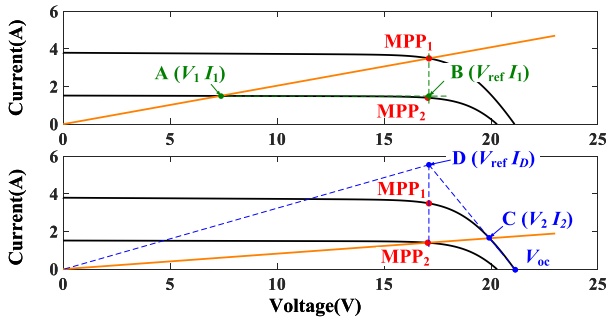

FIGURE 27. Determination of I_{mpp} by [74].

TABLE 4. Values of β under various irradiance and temperature.

No.	Solar Irradiance	temperature	β
1	$1000W/m^2$	$45°C$	-15.4505
2	$1000W/m^2$	$5°C$	-18.3431
3	$300W/m^2$	$45°C$	-15.9587
4	$300W/m^2$	$5°C$	-19.0214

close to MPP_2. After this, the P&o method will be used to find the real MPP

When the solar irradiance is increased, the operating point moves from MPP_2 to point C (V_2, I_2). Then, by applying the trigonometry rule, I_D can be derived as:

$$\frac{V_2 - V_{mpp2}}{I_D - I_2} = \frac{V_{oc}^* - V_{mpp2}}{I_D} \tag{40}$$

Rearrange (40), and obtain (41)

$$I_D = \frac{V_{oc}^* - V_{mpp2}}{V_{oc}^* - V_2} \times I_2 \tag{41}$$

Although the obtained I_D is much higher than the corresponding I_{mpp}, it does not affect the calculation of V_{ref}.

E. BETA METHOD

Beta method is a very unique MPPT method. Unlike the aforementioned MPPT methods, an intermediate variable, β, rather than power or voltage is used to track the MPP The theory of the Beta method is illustrated in [75] and the intermediate variable β is given as:

$$\beta = \ln\left(\frac{I_{pv}}{V_{pv}}\right) - c \times V_{pv} \tag{42}$$

where $c = q/(N_s \eta k T)$ is the diode constant.

Firstly, the Beta method is required to determine the bounding range of β, namely β_{min}, β_{max}. The range of β depends on the working environment of the PV system. TABLE 4 demonstrates working environmental conditions and the calculated magnitudes of β. The relationship among β, voltage and power under various irradiation and temperature conditions is indicated in FIGURE 28. From TABLE 4 and FIGURE 28, the range of β is determined as $\beta_{min} = -19.02$ and $\beta_{max} = -15.45$.

After that, the Beta method will detect whether the value of β is within the range of β. If the value of β is within the range

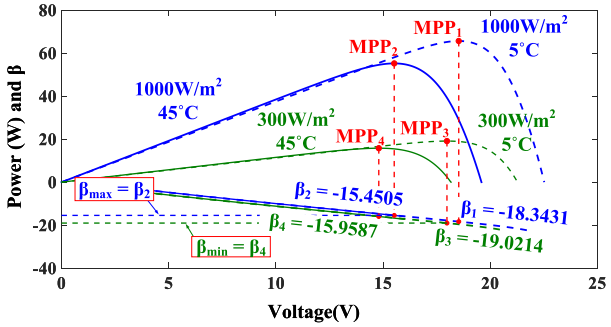

FIGURE 28. Determination of β range based on the working environmental conditions.

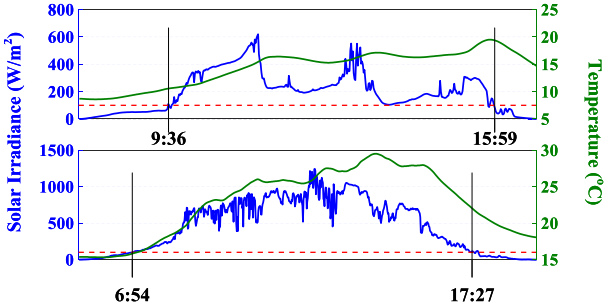

FIGURE 29. Meteorological data of the HSU in the daytime: in 2015/01/19 (top) and 2015/07/31 (bottom).

of β, it means that the operating point is close the MPP. Thus, the fixed step P&O method can be used to exactly locate the MPP. Otherwise, if the value of β is out of this range, it means that the operating point is far from the MPP. Hence, a variable step ΔD is used, which can be expressed as:

$$\Delta D = N \times \left(\beta(k) - \beta_g\right) \tag{43}$$

where $\beta(k)$ is the instantaneous value of β, N is the scaling factor, and β_g is a guiding parameter.

The previous simulation and experimental results from [76], [77] validate the effectiveness of Beta method. However, there are two problems which are not resolved in [76], [77]:

- How to validate the bounding range of β;
- How to optimize the parameters, such as N and β_g.

1) VALIDATION OF BOUNDING RANGE

In [37], the meteorological data of Humboldt State University (HSU) and University of Nevada, Las Vegas (UNLV) are used to validate the effectiveness of bounding range. FIGURE 29 and FIGURE 30 shows the meteorological data of HSU and UNLV, respectively. The solar irradiance in the HSU changes more frequently and dramatically than that of the UNLV due to the different meteorological conditions. The range of temperature in both locations is within 5°C and 40°C. Since the power under 100W/m^2 is negligible, only the meteorological data with solar irradiance higher than 100W/m^2 is considered.

FIGURE 31 and FIGURE 32 illustrate the corresponding simulated values of power and β at the MPP in HSU

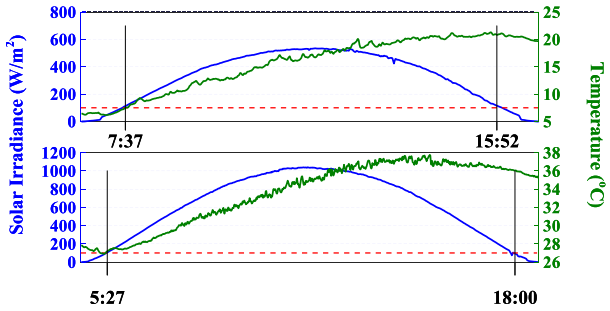

FIGURE 30. Meteorological data of the UNLV in the daytime in 2015/01/16 (top) and 2015/07/24 (bottom).

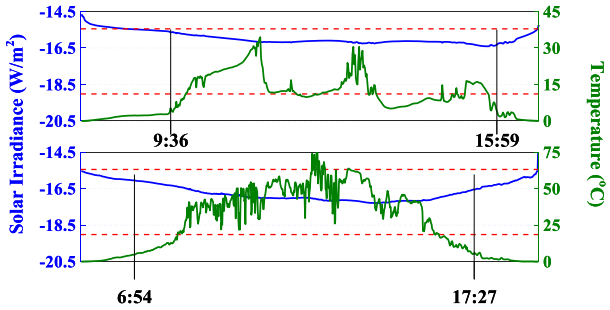

FIGURE 31. The corresponding simulated value of power and β at the MPP in HSU in 2015/01/19 (top) and 2015/07/31 (bottom).

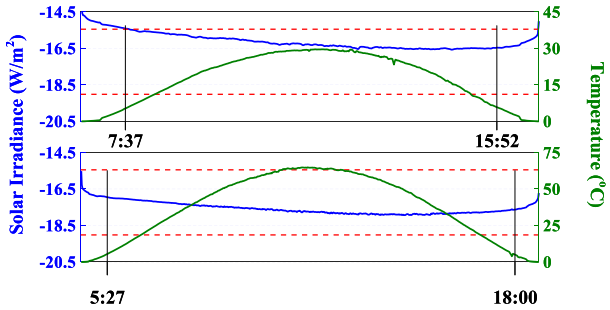

FIGURE 32. The corresponding simulated value of power and β at the MPP in UNLV in 2015/01/16 (top) and 2015/07/24 (bottom).

and UNLV, respectively. Since the solar irradiance has more remarkable effect on the generated power than temperature, it can be seen that the simulated power has a similar trend as the solar irradiance. However, the temperature has more remarkable effect on the values of β compared to the solar irradiance. Therefore, the trends of temperature and the values of β are the similar. Furthermore, during the daytime, the corresponding simulated values of β generally stays within the range between β_{min} and β_{max}. It proves that the set of β parameters in TABLE 4 and FIGURE 28 are able to work in the whole year under the real weather condition.

2) OPTIMIZATION OF CORRESPONDING PARAMETERS

There are two parameters needed to be tuned: one is scaling factor and the other is β_g. Generally, tuning these parameters is based on trial-and error [78]. In [78], adaptive scaling factor Beta (ASF-Beta) method is proposed. Compared to (43),

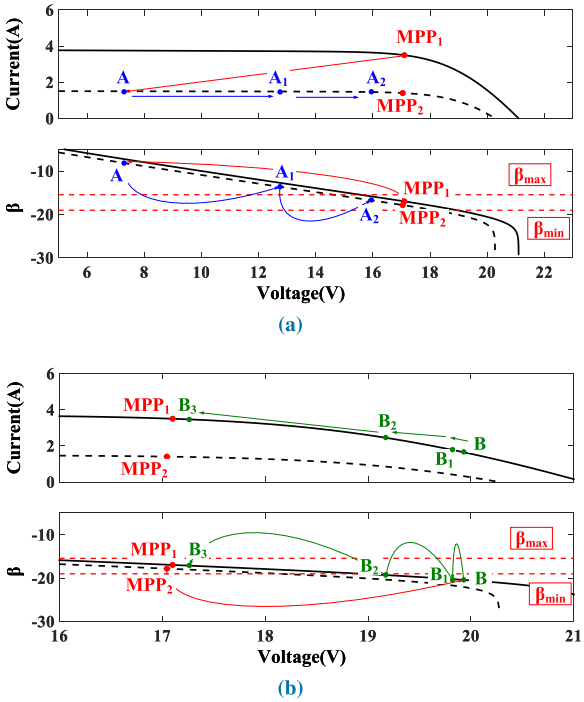

FIGURE 33. Operational principle of the ASF-Beta method. (a) Solar irradiance is decreased; (b) solar irradiance is increased.

the guiding parameter β_g is removed and the step size can updated adaptively as

$$\Delta D = \begin{cases} N \times (\beta_a(k) - \beta_{min}), & \beta_a(k) > \beta_{max} \quad (44a) \\ N \times (\beta_a(k) - \beta_{max}), & \beta_a(k) < \beta_{min} \quad (44b) \end{cases}$$

where (44a) and (44b) refer to the step size when the solar irradiance is decreased and increased, respectively. Then, the adaptive scaling factor N shown in (44) is derived by:

$$N = \begin{cases} 1, & \beta(k-1) < \beta_{max} \quad (45a) \\ \dfrac{\beta(k) - \beta_{min}}{\beta(k-1) - \beta(k)}, & \beta(k-1) > \beta_{max} \quad (45b) \end{cases}$$

$$N = \begin{cases} 1, & \beta(k-1) > \beta_{min} \quad (46a) \\ \dfrac{\beta(k) - \beta_{max}}{\beta(k-1) - \beta(k)}, & \beta(k-1) < \beta_{min} \quad (46b) \end{cases}$$

where (45) and (46) refer to the changes of N when the solar irradiance is decreased and increased, respectively; $\beta(k-1)$ refers to the previous value of β.

The operational principle of the ASF-Beta method is demonstrated in FIGURE 33. When the solar irradiance is suddenly decreased, the operating point moves from MPP_1 to point A, as shown in FIGURE 33 (a). At this time, the algorithm detects that the present operating point is out of the bounding range while the previous one is not. ΔD and N are calculated by (44a) and (45a), respectively. Then, the operating point moves to point A_1. In the next round, ΔD and N are calculated by (44a) and (45b), respectively. The operating point moves to point A_2, which is within the bounding range. After this, the P&O method is used to track the exact location of the MPP. It should be noted that similar procedure is

TABLE 5. Summarization on the evolution of the reviewed MPPT methods.

Method	Ref.	Drawbacks	Solutions	Ref.
P&O and INC	[30]-[34]	Steady-state oscillations Simultaneous optimization Drift conditions	Zero-oscillations Methods Variable-step Size Methods Drift-free Methods	[35]-[37] [38]-[44] [35],[45]-[46]
FLC	[47]–[54]	Design difficulties	Design Simplification Parameter Optimization	[54] [55]-[62]
Curve-fitting	[63]–[64]	Requirement on special measurement points	Parabolic Prediction Parameter Estimation	[65]-[67] [68]-[70]
MPP-locus	[71]	Insufficient tracking procedure	Expression of Voltage Line Maintain at Voltage Line	[72]-[73] [74]
Beta	[75]–[77]	Lack of guideline on parameters	Bounding Range Validation Parameters Optimization	[78] [78]

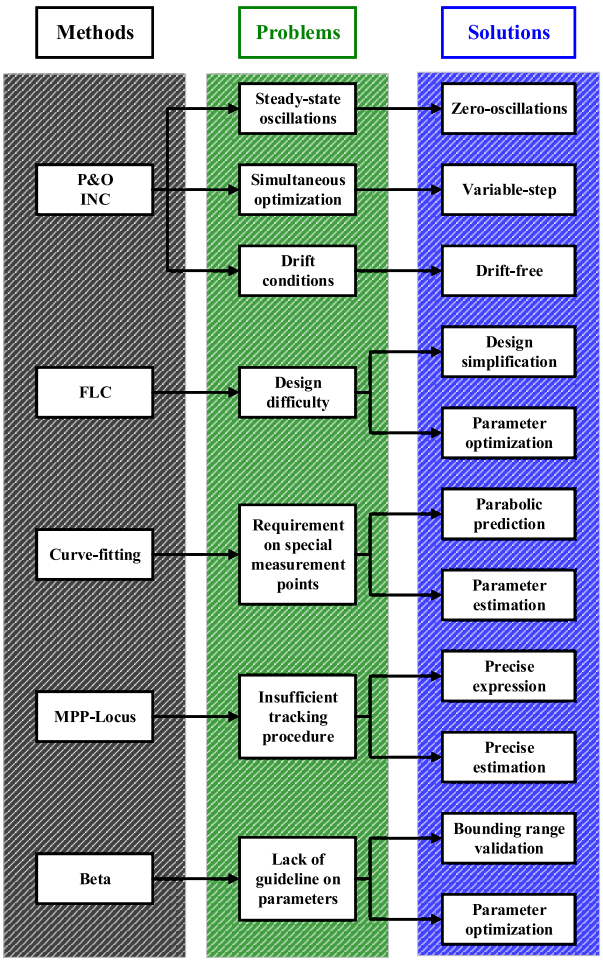

FIGURE 34. Summarization on the evolution of the reviewed MPPT methods.

conducted when the solar irradiance is increased, which will not be discussed here.

From FIGURE 33 (a) and (b), it is clearly seen that the step size is adaptively tuned. The effectiveness of ASF-Beta method is validated by simulation and experimental results in [78].

Finally, the evolution of the reviewed MPPT methods is summarized in FIGURE 34 and TABLE 5.

IV. CONCLUSION AND FUTURE WORK

In this paper, many MPPT methods are reviewed and classified into five groups. The operational principles of these MPPT methods are comprehensively studied. Many efforts have been made to improve the conventional MPPT methods. An overview on the relevance and evolution of these MPPT methods are also revealed. It can be seen that the research on MPPT methods. Therefore, future work is suggested to modify MPPT to work under the PSC.

REFERENCES

[1] EPIA. *Global Market Outlook 2018–2022*. Accessed: Jul. 2018. [Online]. Available: http://solarpowereurope.org/reports/global-market-outlook-2018/?L=994
[2] F.-F. Yang and X.-G. Zhao, "Policies and economic efficiency of China's distributed photovoltaic and energy storage industry," *Energy*, vol. 154, pp. 221–230, Jul. 2018.
[3] R. A. Mastromauro, M. Liserre, and A. Dell'Aquila, "Control issues in single-stage photovoltaic systems: MPPT, current and voltage control," *IEEE Trans. Ind. Informat.*, vol. 8, no. 2, pp. 241–254, May 2012.
[4] T. Esram and P. L. Chapman, "Comparison of photovoltaic array maximum power point tracking techniques," *IEEE Trans. Energy Convers.*, vol. 22, no. 2, pp. 439–449, Jun. 2007.
[5] B. Subudhi and R. Pradhan, "A comparative study on maximum power point tracking techniques for photovoltaic power systems," *IEEE Trans. Sustain. Energy*, vol. 4, no. 1, pp. 89–98, Jan. 2013.
[6] P. Joshi and S. Arora, "Maximum power point tracking methodologies for solar PV systems—A review," *Renew. Sustain. Energy Rev.*, vol. 70, pp. 1154–1177, Apr. 2017.
[7] M. A. Ramli, S. Twaha, K. Ishaque, and Y. A. Al-Turki, "A review on maximum power point tracking for photovoltaic systems with and without shading conditions," *Renew. Sustain. Energy Rev.*, vol. 67, pp. 144–159, Jan. 2017.
[8] J. P. Ram, T. S. Babu, and N. Rajasekar, "A comprehensive review on solar PV maximum power point tracking techniques," *Renew. Sustain. Energy Rev.*, vol. 67, pp. 826–847, Jan. 2017.
[9] M. A. Danandeh and S. M. G. Mousavi, "Comparative and comprehensive review of maximum power point tracking methods for PV cells," *Renew. Sustain. Energy Rev.*, vol. 82, pp. 2743–2767, Feb. 2018.
[10] X. Li and H. Wen, "Evaluation of different maximum power point tracking techniques by using EN 50530 dynamic test standard," in *Proc. IEEE Int. Conf. Power Electron., Drives Energy Syst. (PEDES)*, Dec. 2016, pp. 1–6.
[11] X. Li, H. Wen, and Y. Hu, "Evaluation of different maximum power point tracking (MPPT) techniques based on practical meteorological data," in *Proc. IEEE Int. Conf. Renew. Energy Res. Appl. (ICRERA)*, Nov. 2016, pp. 696–701.
[12] Y. Mahmoud, M. Abdelwahed, and E. F. El-Saadany, "An enhanced MPPT method combining model-based and heuristic techniques," *IEEE Trans. Sustain. Energy*, vol. 7, no. 2, pp. 576–585, Apr. 2016.

[13] E. Bianconi, J. Calvente, R. Giral, E. Mamarelis, G. Petrone, C. A. Ramos-Paja, G. Spagnuolo, and M. Vitelli, "A fast current-based MPPT technique employing sliding mode control," *IEEE Trans. Ind. Electron.*, vol. 60, no. 3, pp. 1168–1178, Mar. 2013.

[14] Y. Hu, W. Cao, J. Wu, B. Ji, and D. Holliday, "Thermography-based virtual MPPT scheme for improving PV energy efficiency under partial shading conditions," *IEEE Trans. Power Electron.*, vol. 29, no. 11, pp. 5667–5672, Nov. 2014.

[15] N. Femia, G. Petrone, G. Spagnuolo, and M. Vitelli, *Power Electronics and Control Techniques for Maximum Energy Harvesting in Photovoltaic Systems*. Boca Raton, FL, USA: CRC Press, 2012.

[16] W. Xiao, *Photovoltaic Power System: Modeling, Design, and Control*. Hoboken, NJ, USA: Wiley, 2017.

[17] M. G. Villalva, J. R. Gazoli, and E. R. Filho, "Comprehensive approach to modeling and simulation of photovoltaic arrays," *IEEE Trans. Power Electron.*, vol. 24, no. 5, pp. 1198–1208, May 2009.

[18] J. Bai, Y. Cao, Y. Hao, Z. Zhang, S. Liu, and F. Cao, "Characteristic output of PV systems under partial shading or mismatch conditions," *Sol. Energy*, vol. 112, pp. 41–54, Feb. 2015.

[19] T. L. Nguyen and K.-S. Low, "A global maximum power point tracking scheme employing DIRECT search algorithm for photovoltaic systems," *IEEE Trans. Ind. Electron.*, vol. 57, no. 10, pp. 3456–3467, Oct. 2010.

[20] N. A. Ahmed and M. Miyatake, "A novel maximum power point tracking for photovoltaic applications under partially shaded insolation conditions," *Electr. Power Syst. Res.*, vol. 78, no. 5, pp. 777–784, 2008.

[21] R. Ramaprabha, M. Balaji, and B. Mathur, "Maximum power point tracking of partially shaded solar PV system using modified Fibonacci search method with fuzzy controller," *Int. J. Elect. Power Energy Syst.*, vol. 43, no. 1, pp. 754–765, 2012.

[22] E. Koutroulis and F. Blaabjerg, "A new technique for tracking the global maximum power point of PV arrays operating under partial-shading conditions," *IEEE J. Photovolt.*, vol. 2, no. 2, pp. 184–190, Apr. 2012.

[23] X. Li, H. Wen, G. Chu, Y. Hu, and L. Jiang, "A novel power-increment based GMPPT algorithm for PV arrays under partial shading conditions," *Sol. Energy*, vol. 169, pp. 353–361, Jul. 2018.

[24] G. Carannante, C. Fraddanno, M. Pagano, and L. Piegari, "Experimental performance of MPPT algorithm for photovoltaic sources subject to inhomogeneous insolation," *IEEE Trans. Ind. Electron.*, vol. 56, no. 11, pp. 4374–4380, Nov. 2009.

[25] Y.-H. Ji, D.-Y. Jung, J.-G. Kim, J.-H. Kim, T.-W. Lee, and C.-Y. Won, "A real maximum power point tracking method for mismatching compensation in PV array under partially shaded conditions," *IEEE Trans. Power Electron.*, vol. 26, no. 4, pp. 1001–1009, Apr. 2011.

[26] H. Patel and V. Agarwal, "Maximum power point tracking scheme for PV systems operating under partially shaded conditions," *IEEE Trans. Ind. Electron.*, vol. 55, no. 4, pp. 1689–1698, Apr. 2008.

[27] K. S. Tey and S. Mekhilef, "Modified incremental conductance algorithm for photovoltaic system under partial shading conditions and load variation," *IEEE Trans. Ind. Electron.*, vol. 61, no. 10, pp. 5384–5392, Oct. 2014.

[28] K. Chen, S. Tian, Y. Cheng, and L. Bai, "An improved MPPT controller for photovoltaic system under partial shading condition," *IEEE Trans. Sustain. Energy*, vol. 5, no. 3, pp. 978–985, Jul. 2014.

[29] Y. Wang, Y. Li, and X. Ruan, "High-accuracy and fast-speed MPPT methods for PV string under partially shaded conditions," *IEEE Trans. Ind. Electron.*, vol. 63, no. 1, pp. 235–245, Jan. 2016.

[30] N. Femia, G. Petrone, G. Spagnuolo, and M. Vitelli, "Optimization of perturb and observe maximum power point tracking method," *IEEE Trans. Power Electron.*, vol. 20, no. 4, pp. 963–973, Jul. 2005.

[31] A. Safari and S. Mekhilef, "Simulation and hardware implementation of incremental conductance MPPT with direct control method using Cuk converter," *IEEE Trans. Ind. Electron.*, vol. 58, no. 4, pp. 1154–1161, Apr. 2011.

[32] M. A. Elgendy, B. Zahawi, and D. J. Atkinson, "Assessment of perturb and observe MPPT algorithm implementation techniques for PV pumping applications," *IEEE Trans. Sustain. Energy*, vol. 3, no. 1, pp. 21–33, Jan. 2012.

[33] M. A. Elgendy, B. Zahawi, and D. J. Atkinson, "Operating characteristics of the P&O algorithm at high perturbation frequencies for standalone PV systems," *IEEE Trans. Energy Convers.*, vol. 30, no. 1, pp. 189–198, Mar. 2015.

[34] M. A. Elgendy, B. Zahawi, and D. J. Atkinson, "Assessment of the incremental conductance maximum power point tracking algorithm," *IEEE Trans. Sustain. Energy*, vol. 4, no. 1, pp. 108–117, Jan. 2013.

[35] T. K. Soon and S. Mekhilef, "Modified incremental conductance MPPT algorithm to mitigate inaccurate responses under fast-changing solar irradiation level," *Sol. Energy*, vol. 101, pp. 333–342, Mar. 2014.

[36] F. Paz and M. Ordonez, "Zero oscillation and irradiance slope tracking for photovoltaic MPPT," *IEEE Trans. Ind. Electron.*, vol. 61, no. 11, pp. 6138–6147, Nov. 2014.

[37] X. Li, H. Wen, L. Jiang, Y. Hu, and C. Zhao, "An improved beta method with autoscaling factor for photovoltaic system," *IEEE Trans. Ind. Appl.*, vol. 52, no. 5, pp. 4281–4291, Sep./Oct. 2016.

[38] F. Liu, S. Duan, B. Liu, and Y. Kang, "A variable step size INC MPPT method for PV systems," *IEEE Trans. Ind. Electron.*, vol. 55, no. 7, pp. 2622–2628, Jul. 2008.

[39] A. Pandey, N. Dasgupta, and A. Mukerjee, "High-performance algorithms for drift avoidance and fast tracking in solar MPPT system," *IEEE Trans. Energy Convers.*, vol. 23, no. 2, pp. 681–689, Jun. 2008.

[40] F. Zhang, K. Thanapalan, A. Procter, S. Carr, and J. Maddy, "Adaptive hybrid maximum power point tracking method for a photovoltaic system," *IEEE Trans. Energy Convers.*, vol. 28, no. 2, pp. 353–360, Jun. 2013.

[41] A. Ahmed, L. Ran, S. Moon, and J.-H. Park, "A fast PV power tracking control algorithm with reduced power mode," *IEEE Trans. Energy Convers.*, vol. 28, no. 3, pp. 565–575, Sep. 2013.

[42] Q. Mei, M. Shan, L. Liu, and J. M. Guerrero, "A novel improved variable step-size incremental-resistance MPPT method for PV systems," *IEEE Trans. Ind. Electron.*, vol. 58, no. 6, pp. 2427–2434, Jun. 2011.

[43] W. Xiao and W. G. Dunford, "A modified adaptive hill climbing MPPT method for photovoltaic power systems," in *Proc. IEEE 35th Annu. Power Electron. Spec. Conf. (PESC)*, vol. 3, Jun. 2004, pp. 1957–1963.

[44] Y.-T. Chen, Z.-H. Lai, and R.-H. Liang, "A novel auto-scaling variable step-size MPPT method for a PV system," *Sol. Energy*, vol. 102, pp. 247–256, Apr. 2014.

[45] D. Sera, R. Teodorescu, J. Hantschel, and M. Knoll, "Optimized maximum power point tracker for fast-changing environmental conditions," *IEEE Trans. Ind. Electron.*, vol. 55, no. 7, pp. 2629–2637, Jul. 2008.

[46] M. Killi and S. Samanta, "Modified perturb and observe MPPT algorithm for drift avoidance in photovoltaic systems," *IEEE Trans. Ind. Electron.*, vol. 62, no. 9, pp. 5549–5559, Sep. 2015.

[47] B. N. Alajmi, K. H. Ahmed, S. J. Finney, and B. W. Williams, "Fuzzy-logic-control approach of a modified hill-climbing method for maximum power point in microgrid standalone photovoltaic system," *IEEE Trans. Power Electron.*, vol. 26, no. 4, pp. 1022–1030, Apr. 2011.

[48] A. Messai, A. Mellit, A. M. Pavan, A. Guessoum, and H. Mekki, "FPGA-based implementation of a fuzzy controller (MPPT) for photovoltaic module," *Energy Convers. Manage.*, vol. 52, no. 7, pp. 2695–2704, 2011.

[49] A. Al Nabulsi and R. Dhaouadi, "Efficiency optimization of a DSP-based standalone PV system using fuzzy logic and dual-MPPT control," *IEEE Trans. Ind. Informat.*, vol. 8, no. 3, pp. 573–584, Aug. 2012.

[50] M. M. Algazar, H. Al-Monier, H. A. El-Halim, and M. E. E. K. Salem, "Maximum power point tracking using fuzzy logic control," *Int. J. Elect. Power Energy Syst.*, vol. 39, no. 1, pp. 21–28, 2012.

[51] A. El Khateb, N. Abd Rahim, J. Selvaraj, and M. N. Uddin, "Fuzzy-logic-controller-based SEPIC converter for maximum power point tracking," *IEEE Trans. Ind. Appl.*, vol. 50, no. 4, pp. 2349–2358, Jul. 2014.

[52] M. A. A. M. Zainuri, M. A. M. Radzi, A. C. Soh, and N. A. Rahim, "Development of adaptive perturb and observe-fuzzy control maximum power point tracking for photovoltaic boost dc-dc converter," *IET Renew. Power Gener.*, vol. 8, no. 2, pp. 183–194, Mar. 2014.

[53] S. Tang, Y. Sun, Y. Chen, Y. Zhao, Y. Yang, and W. Szeto, "An enhanced MPPT method combining fractional-order and fuzzy logic control," *IEEE J. Photovolt.*, vol. 7, no. 2, pp. 640–650, Mar. 2017.

[54] X. Li, H. Wen, Y. Hu, and L. Jiang, "A novel beta parameter based fuzzy-logic controller for photovoltaic MPPT application," *Renew. Energy*, vol. 130, pp. 416–427, Jan. 2019.

[55] M. Veerachary, T. Senjyu, and K. Uezato, "Feedforward maximum power point tracking of PV systems using fuzzy controller," *IEEE Trans. Aerosp. Electron. Syst.*, vol. 38, no. 3, pp. 969–981, Jul. 2002.

[56] M. Veerachary, T. Senjyu, and K. Uezato, "Neural-network-based maximum-power-point tracking of coupled-inductor interleaved-boost-converter-supplied PV system using fuzzy controller," *IEEE Trans. Ind. Electron.*, vol. 50, no. 4, pp. 749–758, Aug. 2003.

[57] E. Karatepe and T. Hiyama, "Artificial neural network-polar coordinated fuzzy controller based maximum power point tracking control under partially shaded conditions," *IET Renew. Power Generat.*, vol. 3, no. 2, pp. 239–253, 2009.
[58] A. Chaouachi, R. M. Kamel, and K. Nagasaka, "A novel multi-model neuro-fuzzy-based MPPT for three-phase grid-connected photovoltaic system," *Sol. Energy*, vol. 84, no. 12, pp. 2219–2229, 2010.
[59] A. Messai, A. Mellit, A. Guessoum, and S. A. Kalogirou, "Maximum power point tracking using a GA optimized fuzzy logic controller and its FPGA implementation," *Sol. Energy*, vol. 85, no. 2, pp. 265–277, 2011.
[60] A. A. S. Mohamed, A. Berzoy, and O. A. Mohammed, "Design and hardware implementation of FL-MPPT control of PV systems based on GA and small-signal analysis," *IEEE Trans. Sustain. Energy*, vol. 8, no. 1, pp. 279–290, Jan. 2017.
[61] L. K. Letting, J. L. Munda, and Y. Hamam, "Optimization of a fuzzy logic controller for PV grid inverter control using S-function based PSO," *Sol. Energy*, vol. 86, pp. 1689–1700, Jun. 2012.
[62] N. Priyadarshi, S. Padmanaban, P. K. Maroti, and A. Sharma, "An extensive practical investigation of FPSO-based MPPT for grid integrated PV system under variable operating conditions with anti-islanding protection," *IEEE Syst. J.*, vol. 13, no. 2, pp. 1861–1871, Jun. 2019.
[63] H. Saleem and S. Karmalkar, "An analytical method to extract the physical parameters of a solar cell from four points on the illuminated $J-V$ curve," *IEEE Electron Device Lett.*, vol. 30, no. 4, pp. 349–352, Apr. 2009.
[64] J.-C. Wang, Y.-L. Su, J.-C. Shieh, and J.-A. Jiang, "High-accuracy maximum power point estimation for photovoltaic arrays," *Sol. Energy Mat. Sol. Cells*, vol. 95, no. 3, pp. 843–851, 2011.
[65] N. Femia, D. Granozio, G. Petrone, G. Spagnuolo, and M. Vitelli, "Predictive adaptive MPPT perturb and observe method," *IEEE Trans. Aerosp. Electron. Syst.*, vol. 43, no. 3, pp. 934–950, Jul. 2007.
[66] F.-S. Pai and R.-M. Chao, "A new algorithm to photovoltaic power point tracking problems with quadratic maximization," *IEEE Trans. Energy Convers.*, vol. 25, no. 1, pp. 262–264, Mar. 2010.
[67] F.-S. Pai, R.-M. Chao, S. H. Ko, and T.-S. Lee, "Performance evaluation of parabolic prediction to maximum power point tracking for PV array," *IEEE Trans. Sustain. Energy*, vol. 2, no. 1, pp. 60–68, Jan. 2011.
[68] J.-H. Teng, W.-H. Huang, T.-A. Hsu, and C.-Y. Wang, "Novel and fast maximum power point tracking for photovoltaic generation," *IEEE Trans. Ind. Electron.*, vol. 63, no. vol. 8, pp. 4955–4966, Apr. 2016.
[69] J. M. Blanes, F. J. Toledo, S. Montero, and A. Garrigos, "In-site real-time photovoltaic I-V curves and maximum power point estimator," *IEEE Trans. Power Electron.*, vol. 28, no. 3, pp. 1234–1240, Mar. 2013.
[70] M. J. Z. Zadeh and S. H. Fathi, "A new approach for photovoltaic arrays modeling and maximum power point estimation in real operating conditions," *IEEE Trans. Ind. Electron.*, vol. 64, no. 12, pp. 9334–9343, Dec. 2017.
[71] M. Sokolov and D. Shmilovitz, "A modified MPPT scheme for accelerated convergence," *IEEE Trans. Energy Convers.*, vol. 23, no. 4, pp. 1105–1107, Dec. 2008.
[72] V. V. R. Scarpa, S. Buso, and G. Spiazzi, "Low-complexity MPPT technique exploiting the PV module MPP locus characterization," *IEEE Trans. Ind. Electron.*, vol. 56, no. 5, pp. 1531–1538, May 2009.
[73] Y.-H. Liu and J.-W. Huang, "A fast and low cost analog maximum power point tracking method for low power photovoltaic systems," *Sol. Energy*, vol. 85, no. 11, pp. 2771–2780, 2011.
[74] T. K. Soon and S. Mekhilef, "A fast-converging MPPT technique for photovoltaic system under fast-varying solar irradiation and load resistance," *IEEE Trans Ind. Informat.*, vol. 11, no. 1, pp. 176–186, Feb. 2015.
[75] S. Jain and V. Agarwal, "A new algorithm for rapid tracking of approximate maximum power point in photovoltaic systems," *IEEE Power Electron Lett.*, vol. 2, no. 1, pp. 16–19, Mar. 2004.
[76] M. A. G. de Brito, L. Galotto, L. P. Sampaio, G. E. de Azevedo e Melo, and C. A. Canesin, "Evaluation of the main MPPT techniques for photovoltaic applications," *IEEE Trans. Ind. Electron.*, vol. 60, no. 3, pp. 1156–1167, Mar. 2013.
[77] S. Jain and V. Agarwal, "Comparison of the performance of maximum power point tracking schemes applied to single-stage grid-connected photovoltaic systems," *IET Electr. Power Appl.*, vol. 1, no. 5, pp. 753–762, Sep. 2007.
[78] X. Li, H. Wen, L. Jiang, W. Xiao, Y. Du, and C. Zhao, "An improved MPPT method for PV system with fast-converging speed and zero oscillation," *IEEE Trans. Ind. Appl.*, vol. 52, no. 6, pp. 5051–5064, Nov. 2016.

XINGSHUO LI (S'16) received the B.S. degree in computer science from Zhengzhou University, Zhengzhou, China, in 2012, the M.S. degree (Hons.) in sustainable energy technology from Xi'an Jiaotong-Liverpool University, Suzhou, China, in 2015, and the Ph.D. degree from the University of Liverpool, Liverpool, U.K., in 2019.

He is currently a Lecturer with the School of Electrical and Automation Engineering, Nanjing Normal University, Nanjing, China. His research interests include renewable energy technology and distributed generation, especially ancillary service, power forecasting, and fault diagnosis in photovoltaic systems.

QI WANG received the B.S., M.S., and Ph.D. degrees in electrical engineering from the Harbin Institute of Technology, Harbin, China, in 1998, 2003, and 2008, respectively.

From September 2010 to January 2013, she held a postdoctoral position at Hohai University, Nanjing, China. From March 2013 to September 2013, she was a Visiting Scholar with Northumbria University, Newcastle, U.K. Since 1998, she has been with the School of Electrical and Automation Engineering, Nanjing Normal University, Nanjing, where she is currently an Associate Professor. Her current research interests include optimization of power systems, renewable energy generation, and application of power electronics in the power systems.

HUIQING WEN (M'13–SM'18) received the B.S. and M.S. degrees in electrical engineering from Zhejiang University, Hangzhou, China, in 2002 and 2006, respectively, and the Ph.D. degree in electrical engineering from the Chinese Academy of Sciences, Beijing, China, in 2009.

From 2009 to 2010, he was an Electrical Engineer with the GE (China) Research and Development Center Company Ltd., Shanghai, China. From 2010 to 2011, he was an Engineer with the China Coal Research Institute, Beijing. From 2011 to 2012, he was a Postdoctoral Fellow with the Masdar Institute of Science and Technology, Abu Dhabi, United Arab Emirates. In 2013, he joined the Electrical and Electronic Engineering Department, Xi'an Jiaotong-Liverpool University (XJTLU), Suzhou, China, where he is currently a Senior Associate Professor. He has published more than 100 peer-reviewed technical articles in leading journals/conferences, and he holds over 20 issued/pending patents. His research interests include renewable energy, electric vehicle, power electronics, microgrids, and power semiconductor devices.

Dr. Wen is currently an Associate Editor of IEEE Access, the *International Journal of Photoenergy*, and the *Journal of Power Electronics*.

WEIDONG XIAO (SM'13) received the master's and Ph.D. degrees in electrical engineering from The University of British Columbia, Vancouver, BC, Canada, in 2003 and 2007, respectively.

From 2010 to 2016, he was with the Masdar Institute of Science and Technology, United Arab Emirates. In 2010, he was a Visiting Scholar with the Massachusetts Institute of Technology (MIT), Cambridge, MA, USA, where he was involved in the power interfaces for PV power systems. Prior to the academic career, he was a Research and Development Engineering Manager with MSR Innovations Inc., Canada, focusing on integration, research, optimization, and design of photovoltaic power systems. He is currently an Associate Professor with the School of Electrical and Information Engineering, University of Sydney, Australia. His research interests include photovoltaic power systems, power electronics, dynamic modeling, control engineering, dc systems, and industry applications.

Dr. Xiao is currently an Associate Editor of the IEEE Transactions on Industrial Electronics.